Applied Catalysis B: Environmental 300 (2022) 120731

Contents lists available at ScienceDirect

Applied Catalysis B: Environmental

journal homepage: www.elsevier.com/locate/apcatb

Stabilizing the isolated Pt sites on $PtGa/Al_2O_3$ catalyst via silica coating layers for propane dehydrogenation at low temperature

Peng Wang [a], Jikang Yao [a], Qike Jiang [b], Xinhua Gao [c], Dong Lin [d], Hua Yang [a], Lizhi Wu [a], Yu Tang [a,*], Li Tan [a,*]

[a] Institute of Molecule Catalysis and In-Situ/Operando Studies, College of Chemistry, Fuzhou University, Fuzhou 350108, China
[b] Dalian National Laboratory for Clean Energy, Dalian Institute of Chemical Physics, Chinese Academy of Sciences, 457 Zhongshan Road, Dalian 116023, China
[c] State Key Laboratory of High-Efficiency Utilization of Coal and Green Chemical Engineering, College of Chemistry and Chemical Engineering, Ningxia University, Yinchuan 750021, China
[d] State Key Laboratory of Heavy Oil Processing, China University of Petroleum (East China), Qingdao 266580, China

ARTICLE INFO

Keywords:
Propane
Dehydrogenation
Propylene
Platinum
Metal-support interaction

ABSTRACT

Catalytic conversion of propane to propylene can be achieved by non-oxidative propane dehydrogenation (PDH) by Pt-based catalysts under 550–700 °C. In this work, we report a strategy to decrease the Pt loading amount to only 0.1 wt% for obtaining a stable catalyst via silica coating for high PDH activity at a temperature as low as of 450 °C. The as-prepared 2.5%Si@$PtGa/Al_2O_3$ catalyst shows outstanding catalytic activity (propylene productivity rate 0.5 mol/$g_{cat.}$·h) close to its equilibrium conversion (24.5%) with much better stability (deactivation constant: 0.007 h^{-1}) at 450 °C. The interface between catalyst and silica coating changes the strong metal-support interaction (SMSI) to immobilize the Ga oxide clusters, further tightly anchoring the Pt catalytic sites for PDH process. Moreover, the electronic state of Pt is also influenced by the silica coating layers. This work demonstrates a new method to harnessing the metal-support interaction in catalysis.

1. Introduction

Propylene is one of the most important building blocks for industrial production to many chemical products including polypropylene, which is an essential material to prepare non-woven fabric for personal protection equipment amid global COVID-19 [1–3]. Due to the increasing global demand for propylene, the market price of propylene has been rising accompanied with the booming trend of industrial development [4–8]. Therefore, many efforts have been devoted to the transformation of propane into propylene stimulated by the large scale production of propane by the development of shale-gas extraction [9]. To date, Pt-based catalysts have been extensively used as industrial catalysts for propane direct dehydrogenation (PDH) with a desirable performance in Oleflex process for its longer reaction lifetime and more environmental friendly [10]. However, the wider application is still hampered since the usage of noble metal and catalyst deactivation. Thus, it's still necessary to develop a low cost catalyst for the PDH regarding to utilization of natural gas resources [11–13].

The PDH process is featured by its high endothermicity (ΔH^{θ}_{298} = 124.3 kJ mol^{-1}) [4,14], which requires high reaction temperature (550–700 °C) [15–18]. Such harsh reaction conditions compose a chanllege to the thermal stability of the catalyst. Alkane activation at the lower temperature (<500 °C) has attracted more and more research interest for a series of merits, such as reducing the energy consumption and inhibiting of coking and sintering [19–25]. Considering the thermodynamics equilibrium limitation as the function of temperature for PDH (Fig. S10), realizing the PDH process with good catalytic performance at the lower temperature is an emerging significant challenge. Hence, the exploitation of high-activity catalysts capable of good catalytic performance in PDH reaction at low temperature is quite urgent.

Among those most promising catalysts for PDH reaction, the single-atom Pt catalyst has been wildly investigated and applied for its unique advantages such as the well-defined isolated active sites, distinct and superior catalytic performance [26–30]. The atomic dispersed Pt sites can readily dissociate the first and second C–H bonds of alkanes at low temperature, and minimize the side reactions to coke formation effectively [9,31]. However, due to the high surface Gibbs free energy of isolated Pt active sites, agglomerating and sintering could occur during catalysis, which would further result in catalyst deactivation [32–36]. Many strategies have been developed for rational design of PDH

* Corresponding authors.
E-mail addresses: yu.tang@fzu.edu.cn (Y. Tang), tan@fzu.edu.cn (L. Tan).

https://doi.org/10.1016/j.apcatb.2021.120731
Received 26 June 2021; Received in revised form 25 August 2021; Accepted 14 September 2021
Available online 22 September 2021

catalyst. For example, the post-transition metal elements (e.g. Sn, Zn, Ga, In) have been explored as co-catalyst to improve the dispersion, geometric structure and electronic properties of Pt for increasing the activity, selectivity, stability and anti-coking performance [37–42]. The introduction of co-catalyst species such as Ga could regulate the strong metal-support interaction (SMSI) between metal and oxide support, and further help to maintain the dispersion of Pt species [9,29,36]. On the other hand, the thermal stability of catalyst and the resistance to coke formation can be improved by coating inorganic oxide shells on the catalyst as a physical barrier to prevent the aggregation of Pt species [41, 43,44]. Lu et al. reported that the Pd/Al_2O_3 catalyst surface can be well regulated through depositing controllable Al_2O_3 overcoating [45]. The anti-sintering ability of Pd particles is greatly improved and the adsorption affinity of product molecules on Pd species is weakened due to the confinement effect of Al_2O_3 atomic layers [45].

In this work, we report that the $PtGa/Al_2O_3$ catalyst coated with silica overlayer shows excellent catalytic performance and stability for the PDH reaction at low temperature (450 °C). A series of catalysts with different silica coating amount by introducing controlled silica amount on the catalysts surface (as shown in Scheme 1). The 2.5%Si@PtGa/Al_2O_3 has shown the most stable catalytic activity for PDH at 450 °C. Furthermore, the relationship between the structure and catalytic performance of catalysts have been investigated by inductively coupled plasma optical emission spectrometer (ICP-OES), nitrogen adsorption (BET), high angle annular dark field scanning transmission electron microscopy (HAADF-STEM), aberration corrected transmission electron microscope (AC-TEM), X-ray diffraction (XRD), H_2 temperature programmed reduction (H_2-TPR), NH_3 temperature programmed desorption (NH_3-TPD), X-ray photoelectron spectroscopy (XPS), diffuse reflectance infrared Fourier transform spectrum of CO (DRIFTS-CO), Raman spectrum, thermogravimetric analysis (TGA) and differential scanning calorimetry (TG-DSC). The enhanced catalytic stability is attributed to the stable Pt active sites anchored by the Ga clusters as well as silica layers on the catalyst surface. This work explores alkane catalytic conversion at lower temperature and demonstrates a new method to improve thermal stability of catalyst.

2. Experimental section

2.1. Catalysts preparation

The γ-Al_2O_3 (99.99%, ≤20 nm, Aladdin) was calcined at 700 °C in air for 2 h before using. Nominal 0.1 wt% Pt and 5 wt% Ga supported on γ-Al_2O_3, denoted as $PtGa/Al_2O_3$, was synthesized via co-impregnation using $Pt(NH_3)_4(NO_3)_2$ (Pt, 50% basis, Sigma-Aldrich) and Ga $(NO_3)_3{\cdot}xH_2O$ (99.9%, Aladdin) dissolved in deionized water. After impregnation, the catalysts were dried overnight in oven at 353 K and calcined at 773 K for 3 h under air. The PtGa/HZSM-5 and $PtGa/SiO_2$ were similarly prepared using HZSM-5 (NKF-5D-25–2, $SiO_2/Al_2O_3 = 27$, Nankai University Catalyst Co., Ltd.) and silica (Kaimike Chemical Industry Trade Co., Ltd.) as supports. Pt/Al_2O_3 and Ga/Al_2O_3 catalysts with 0.1 wt% Pt and 5 wt% Ga on γ-Al_2O_3 support were also synthesized by incipient wetness impregnation method for comparison.

Silica coating on catalysts are according to the protocol in literature [46]. Typically, 0.30 g of as-prepared $PtGa/Al_2O_3$, 40 mL of ethanol, and 2 mL of concentrated ammonium hydroxide ($NH_3{\cdot}H_2O$, AR, 25–28%, Sinopharm Chemical Reagent Co., Ltd.) were mixed under continuously stirring. Then, 20 mL of ethanol with desired weight of tetraethyl orthosilicate (TEOS, AR, SiO_2 >=28.4%, Sinopharm Chemical Reagent Co., Ltd.) was introduced into the above mixture by syringe pump at the rate of 40 μL/min. After the mixture was stirred vigorously for another 12 h, the products were obtained by centrifugation. The as-synthesized materials were dried at 353 K and calcined at 623 K in air for 2 h (ramping rate 2 °C·min^{-1}) to obtain x%Si@$PtGa/Al_2O_3$ (x is the weight percent of Si in the overall catalyst). The actual Pt, Ga and Si content is further determined by ICP-OES.

2.2. Catalysts characterizations

Elemental composition of the catalysts was measured on a iCAP 7000 series ICP-OES (Thermo Fisher Scientific, USA). Transmission electron microscopy (TEM) images and HAADF-STEM images were conducted on a FEI Talos F200S G2 microscope at 200 kV (FEI, USA). The chemical components were carried out using a FEI Super-X energy-dispersive spectrum (EDS) system with a collection solid angle above 0.45 srad. XRD measurements were performed using an Ultimate III diffractometer (Rigaku, Japan) with Cu Kα (λ = 1.5406 Å) at 40 kV and 25 mA. The diffraction patterns were between $5° < 2\theta < 90°$ with a scan speed of 10 ° per minute. The surface area and pore structure parameters of catalysts were analyzed by N_2 adsorption-desorption isotherms at 77 K on a Micromeritics ASAP 2020 plus (Micromeritics, USA). Before measurement, the samples were preheated under vacuum at 200 °C for 8 h. The BJH method was used to calculate the mesoporous specific surface areas and volumes of the catalysts at the range of 2–50 nm. The t-plot method was employed to calculate the micropore specific surface areas and volumes. H_2-TPR was conducted on an AutoChem II 2920 chemisorption analyzer (Micromeritics, USA) equipped with a thermal conductivity detector (TCD). Prior to the TPR experiments, 0.1 g of fresh catalyst was pretreated in flowing Ar at 300 °C for 2 h. The temperature was raised from 50° to 800°C under 10% H_2/Ar at a flow of 30 mL min^{-1} at a heating rate of 10 °C min^{-1}. NH_3-TPD was carried out on an AutoChem II 2920 chemisorption analyzer (Micromeritics, USA) equipped with a thermal conductivity detector (TCD) for the detection of NH_3. 0.2 g of the fresh catalyst was pretreated inflowing He at 300 °C

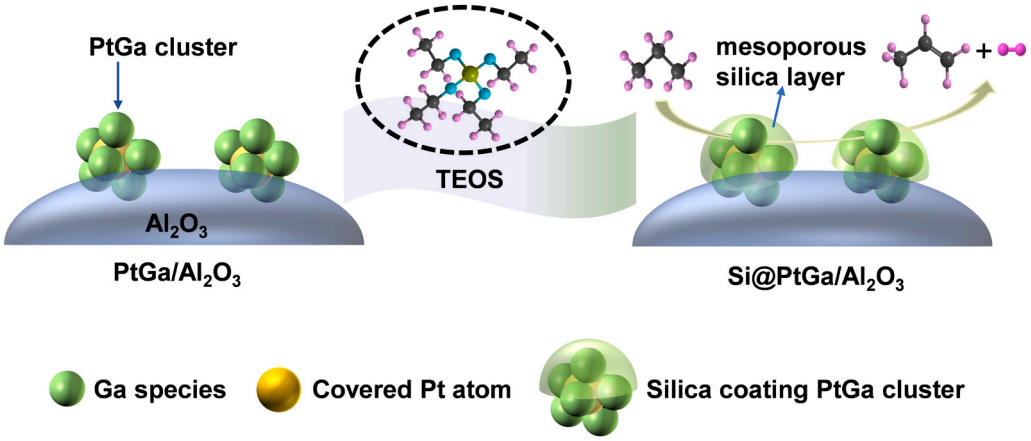

Scheme 1. Demonstration of preparation of Si@$PtGa/Al_2O_3$ catalyst.

for 2 h, and then cooling down to 50 °C for NH_3 adsorption. This was achieved by feeding a constant 10% NH_3/He flow to the reactor for 0.5 h. Then, the flow gas was switched to pure He to remove weakly adsorbed NH_3 until the baseline was stable. The catalyst was heated from 100° to 800°C at a ramping rate of 10 °C min^{-1}.

XPS experiments were carried out on a Thermo Scientific ESCALAB 250 (Thermo Fisher Scientific, USA), and the data was acquired by a monochromatized Al Kα X-ray source (200 W). The binding energies were referenced to the C 1s peak of environmental carbon at 284.6 eV.

The atomic resolution microscopy analysis was performed on a JEM ARM200F thermal-field emission microscope (JOEL, Japan) with a probe spherical aberration (Cs) corrector working at 200 kV.

DRIFTS-CO adsorption experiments were collected on a Nicolet iS50 spectrometer (Thermo Fisher Scientific, USA). Typically, the catalyst was carefully transferred into the Praying mantis in situ cell (Harrick Scientific Product). Before the in situ DRIFTS-CO experiments, the catalyst was purged by Ar flow (>99.99%, 30 mL min^{-1}) for 30 min at 300 °C. After the sample was cooled down to room temperature and collected the background spectrum, the 10% CO/Ar mixture gas was fed into the cell with a flow rate of 20 mL min^{-1} followed by purging with Ar. The DRIFTS-CO spectra was obtained at steady-state by after the subtraction of the background spectra recorded before CO chemisorption.

Raman spectroscopy measurements were carried out on a DXRxi Raman microscope (Thermo Fisher Scientific, USA) with a 532 nm excitation wavelength. The wavenumber values were measured over the range 400–3100 cm^{-1} with an average of 30 scans. TG-DSC analysis was also used to characterize the used catalysts on a STA449F5 Jupiter thermal analyzer (Netzsch, Germany). The temperature was increased from 30° to 800 °C with a heating rate of 5 °C min^{-1}, and the air flow rate was 30 mL min^{-1}.

2.3. Catalytic activity tests

The catalytic experiment of PDH was carried out in a fixed-bed tubular quartz reactor under atmosphere pressure. In a typical test, 0.1 g catalyst (40–60 mesh) diluted with 0.4 g quartz sand (40–60 mesh) was filled into the quartz tube of 6 mm inner diameter. The reactor was raised to 450 °C under pure Ar gas (20 mL min^{-1}) and then kept for 1 h. Then, a mixture of 2.5% propane and 2.5% hydrogen (total 40 mL min^{-1}) were introduced for catalytic activity evaluation [4,34]. The feed and the products were analyzed by an on-line gas chromatograph (Shimazu GC-2014, Japan) equipped with HP-AL/S column (50 m, 0. 53 mm i.d., 15 μm film), one FID detector and one auto sampler. The conversion (X_{C3H8}), selectivity (S_{C3H6}), yield (Y_{C3H6}), propene productivity rate, TOF, carbon balance (CB) and deactivation constant (K_D) [13,18,28,47] for propane were calculated as following:

$$X_{C_3H_8}(\%) = \frac{[C_3H_8]_{in} - [C_3H_8]_{out}}{[C_3H_8]_{in}} \times 100\% \quad (1)$$

$$S_{C_3H_6}(\%) = \frac{[C_3H_6]_{out}}{[C_3H_8]_{in} - [C_3H_8]_{out}} \times 100\% \quad (2)$$

$$Y_{C_3H_6}(\%) = \frac{[C_3H_6]_{out}}{[C_3H_8]_{in}} \times 100\% \quad (3)$$

$$\text{Propene productivity rate}(mol/g_{cat.} \times h) = \frac{F_{(C_3H_8)} \times Y \times 60\ min}{m_{cat.} \times 22.414\ L/mol} \quad (4)$$

$$\text{TOF}(per\ min) = \frac{\text{Number of produced } C_3H_6 \text{ moles}}{\text{Number of actual Pt moles} \times \text{Time}} = \frac{F_{(C_3H_8)} \times Y \times M_w}{m_{cat.} \times W_{Pt} \times 22.414\ L/mol} \quad (5)$$

$$\text{Carbon Balance}\ (\%) = \frac{1/3 \times [CH_4]_{out} + 2/3 \times [C_2H_6]_{out} + 2/3 \times [C_2H_4]_{out} + [C_3H_8]_{out} + [C_3H_6]_{out}}{[C_3H_8]_{in}} \times 100\% \quad (6)$$

$$\text{Deactive constant } K_D = \frac{\ln\left(\frac{100-Y_{end.}}{Y_{end}}\right) - \ln\left(\frac{100-Y_{in.}}{Y_{in}}\right)}{\text{Time}} \quad (7)$$

Where $m_{cat.}$ is the weight of catalysts (g), W_{Pt} is the actual supported percentage of Pt (%), M_w is the molar mass of Pt (g/mol), F is flow rate of hydrocarbon (L/min), Y_{end} is the yield at end of reaction, and Y_{in} is the initial yield.

3. Results and discussion

3.1. the structure of silica coated PtGa/Al_2O_3 catalysts

The morphology of the used PtGa/Al_2O_3 and 2.5%Si@PtGa/Al_2O_3 catalysts were examined by TEM (Fig. 1). The lattice fringes of γ-Al_2O_3 and well definite edges are clearly seen on the non-silica coated PtGa/Al_2O_3 catalyst (Fig. 1a). The interplanar distances marked with white lines are 2.80 and 2.39 Å, which correspond to the (220) and (311) crystal planes of γ-Al_2O_3, respectively. In the contrast, the overall lattice of γ-Al_2O_3 become ambiguous, and the epitaxial growth of amorphous silica layers appears at the edges of the silica coated 2.5%Si@PtGa/Al_2O_3 catalyst (Fig. 1c and d). No crystal grains of Pt or Ga are found in the TEM images of both samples. Moreover, EDS mapping result indicates that Si, Ga, Pt are uniformly dispersed on the surface of catalysts (Fig. 2), suggesting the amorphous silica are coating on the catalyst homogenously.

The actual weight fraction of the catalysts was examined by ICP-OES (Table S1 and S2). The actual Si content increased with the addition of TEOS corresponding to desired Si percentage content. As shown in the XRD patterns of catalysts in Fig. 3, the peaks appearing at 37.5°, 45.7° and 66.8° are attributed to γ-Al_2O_3 phase of the fresh catalysts (PDF# 50-0741) [48]. No diffraction peaks of Ga and Pt are observed on these Pt/Ga based catalysts. It's deduced that the Ga and Pt phases are well distributed on the γ-Al_2O_3 support with extremely small size as atomic clusters. As the increasing of the introduced silica coating, a broad amorphous silica diffraction peak starts to appear on 20%Si@PtGa/Al_2O_3 catalyst at ~23°.

The textural properties of the catalysts were investigated by the N_2 adsorption via BET method (Table 1 and Fig. S1). The typical adsorption-desorption isotherms of type IV indicates that all the catalysts are mesoporous materials accompanied by a small portion of micropores. As shown in Table 1, the surface area of mesopores is slightly increased from 126.3 to 156.3 m^2/g with the decline of micropores volume when Pt and Ga were loaded on Al_2O_3. The average pore width of 2.5%Si@PtGa/Al_2O_3 is 15.8 nm, which is about 31% smaller than

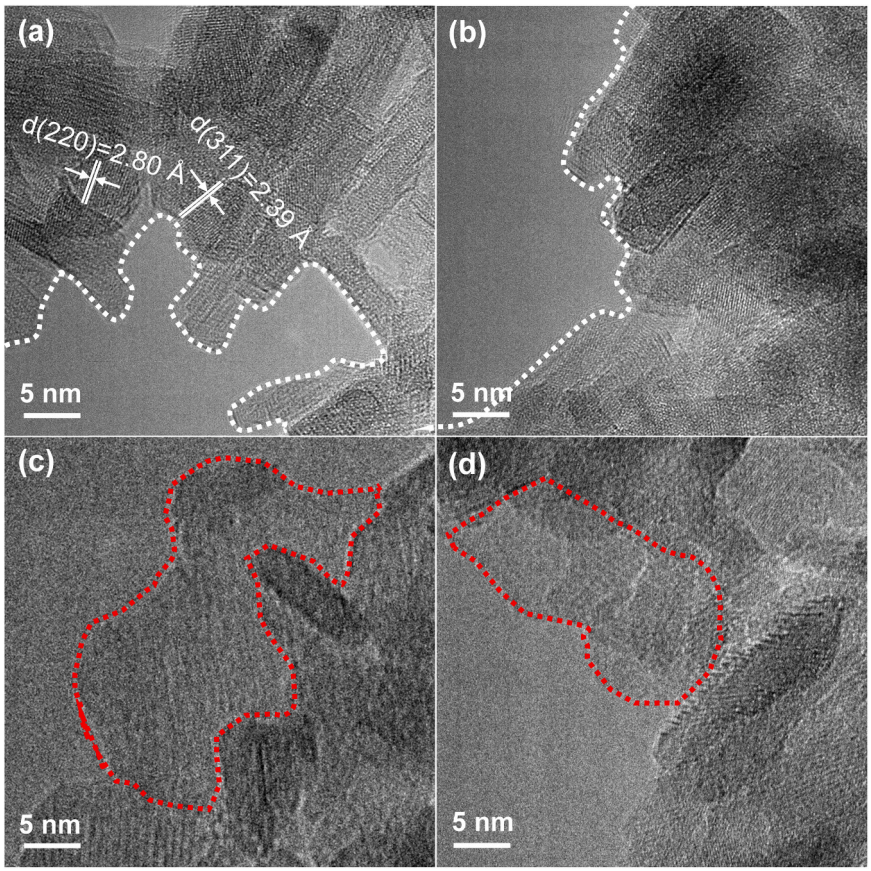

Fig. 1. The TEM images of (a-b) the spent $PtGa/Al_2O_3$ and (c-d) 2.5%Si@$PtGa/Al_2O_3$, The white dash line is the edge of alumina and the red dash line is the epitaxial growth of silica.

that of $PtGa/Al_2O_3$. The surface area and pores volume of mesopores decrease over the silica coated x%Si@$PtGa/Al_2O_3$ catalyst as the silica amounts increasing, which indicates that the introduction of silica into the interior of the mesoporous channel effectively modifies the internal structure of the channel. This phenomenon is also consistent with the average pore width variation (Table S3). However, the excessive amorphous silica phase is generated on the catalysts surface, resulting in the increase of micropores volume. Thus, the results of TEM, EDS, XRD and BET suggest that the introduced amorphous silica layer is well surrounded in the internal and external surfaces of the $PtGa/Al_2O_3$ catalyst.

3.2. Catalytic performance for propane dehydrogenation

As the control experiments, the 0.1 wt% Pt had been loaded onto Al_2O_3 support to obtain highly dispersed Pt catalyst for exposing maximized active sites on the catalyst surface. However, it shows poor catalytic activity with only ~5% C_3H_6 yield and rapid deactivation at the low temperature of 450 °C on Pt/Al_2O_3 catalyst (Fig. S2a). It is inferred that the sintering of Pt may occur during the catalytic process for its weak metal–support interaction between Pt and Al_2O_3 support [9, 30]. Hence, the quantity of surface active sites is decreased, leading to the catalyst deactivation. Controlled experiment shows that γ-Al_2O_3 support is not active for the PDH reaction under the same experimental condition (Fig. S2b).

The Ga was introduced to immobilize the Pt active sites in the $PtGa/Al_2O_3$ catalyst as a promoter. The initial propane conversion is ~9.8% with poor stability (end conversion at 15 h ~4.8%) over Pt/Al_2O_3 catalyst (Fig. S2a), which indicates low performance of monometallic Pt active sites on γ-Al_2O_3 support. In comparison, $PtGa/Al_2O_3$ catalyst shows notably enhanced catalytic performance with 17.4% initial propane conversion (Fig. 4), which is 1.7 times higher than that of Pt/Al_2O_3 catalyst under identical conditions. Although the initial activity of the catalyst has been greatly improved over $PtGa/Al_2O_3$ catalyst, the stability of the catalyst is still poor due to the unstable Pt active sites. It has been reported that the presence of Al-O-Ga sites may promote heterolysis C-H bond activation [49]. However, in this study, the trace amounts of Pt active sites are mainly responsible for catalytic dehydrogenation of propane at low temperature (450 °C), while the monometallic Ga catalyst shows minimum activity at the same reaction condition (Fig. S2c) and the related catalytic activities of different Ga species are discussed in detail in the Supporting information (Fig. S11).

To further improve the stability of Pt active sites, the $PtGa/Al_2O_3$ catalyst was coated by silica layers to regulate its metal-support interaction between Pt and the Al_2O_3 substrate (Scheme 1). For comparison, the catalytic activity test of the 2.5%Si@Pt/Al_2O_3 shows that the initial conversion is 9.2% (end conversion at 15 h ~5.6%) with obvious deactivation (Fig. S3a). The catalytic activities of a series of x% Si@$PtGa/Al_2O_3$ (x = 0, 0.5, 2.5, 5, 20) were evaluated in the PDH reaction at 450 °C, and the results of catalytic activity, deactivation constants and carbon balance are shown in Fig. 4, and Figs. S4–10. It is worth noting that the C_3H_6 selectivity of $PtGa/Al_2O_3$ is 81.6%, while the selectivity is almost above 90% over all x%Si@$PtGa/Al_2O_3$ catalysts. The selectivity to propylene is enhanced by silica coating. The stability of the silica coated catalysts are significantly improved for PDH reaction. It indicates that the environment of Pt active sites may be tuned via the encapsulation of silica shell. Among all the catalysts, the 2.5%Si@$PtGa/Al_2O_3$ shows the best catalytic performance with 21.8% propane conversion and 90.7% propylene selectivity initially, which is very close to its thermal dynamics equilibrium conversion of propane at this reaction condition, which is ~25% at the same reaction condition obtained by HSC thermodynamic simulation (Fig. S12). Meanwhile, it gives the

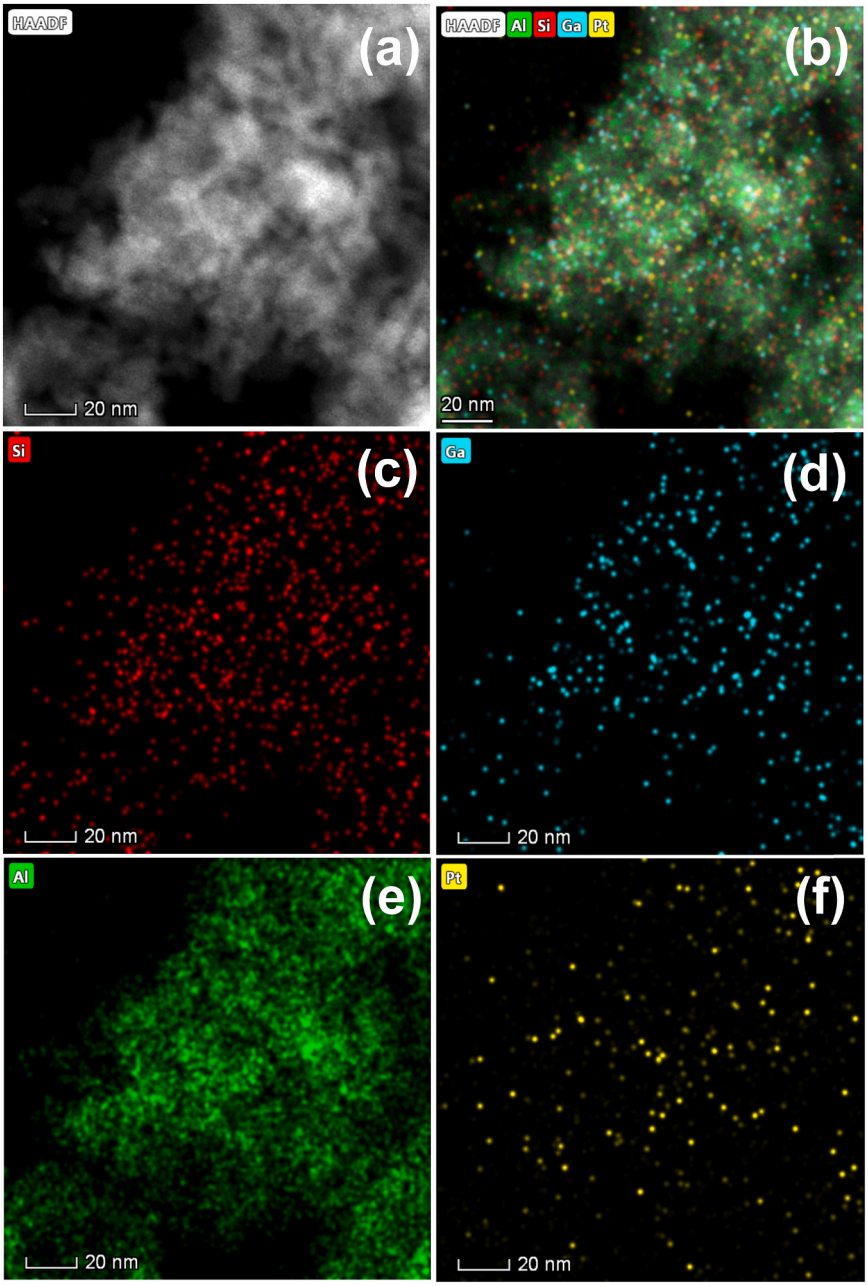

Fig. 2. TEM analysis of the spent 2.5%Si@PtGa/Al_2O_3 catalyst. (a) representative HAADF image, (b-f) corresponding element mapping of Si, Ga, Al, and Pt.

highest propylene productive rate of ~17.82 (min^{-1}) (Table S4–5) with yield of nearly 20% over the 2.5%Si@PtGa/Al_2O_3 catalyst. Hence, the accessibility of reactants to active sites is not hampered by the coated silica layers on the catalyst surface. Moreover, 2.5%Si@PtGa/Al_2O_3 catalyst possesses the lowest deactivation constant of only 0.007 h^{-1} after 34 h reaction time, indicating that the Pt active sites are steady anchored on the substrate via silica coating.

In order to study the influence of oxide interface on the catalytic performance, the PDH reaction was also tested over PtGa/SiO_2 catalyst (Fig. 4 and Fig. S13). However, the PtGa/SiO_2 shows worse catalytic activity with only ~12.0% propane conversion and ~69.5% propylene selectivity than other catalysts. Besides the deactivation constant is as high as ~0.058 h^{-1}, suggesting a poor stability. For comparison, the catalytic stability of the PtGa/2.5%Si@Al_2O_3 catalyst (deactivation constant: 0.022 h^{-1}) is also significantly poor than that of 2.5% Si@PtGa/Al_2O_3 catalyst (deactivation constant: 0.007 h^{-1}), though the catalytic activity (initial conversion of 21.0%) is improved than that of PtGa/Al_2O_3 (initial yield of 17.4%) and further discussion is in the Support Information (Fig. S14). It is noted that the metal-support interaction between the silica and the active sites is extremely weak. Therefore, the formation of stable Pt active sites of 2.5%Si@PtGa/Al_2O_3 catalyst is caused by the interface of SiO_2/Al_2O_3 and the confinement of its encapsulation structure.

3.3. *Reactivity and surface chemistry of the silica coated catalysts*

The reducibility of Pt and Ga in the x%Si@PtGa/Al_2O_3 (x = 0, 0.5, 2.5, 5, 20) and PtGa/SiO_2 catalysts were analyzed by H_2-TPR measurements in Fig. 5(a). No visible reduction peaks below 300 °C can be detected in the all catalysts due to the extremely low Pt loading amount [29]. The TPR result of PtGa/Al_2O_3 catalyst shows barely reduction peak because of the SMSI between Ga and Al_2O_3 [50]. Notely, a distinct broad reduction peak begins to appears at 482 °C for 0.5%Si@PtGa/Al_2O_3, which is assigned to the reduction of Ga^{3+} to Ga^{2+} [51], indicating

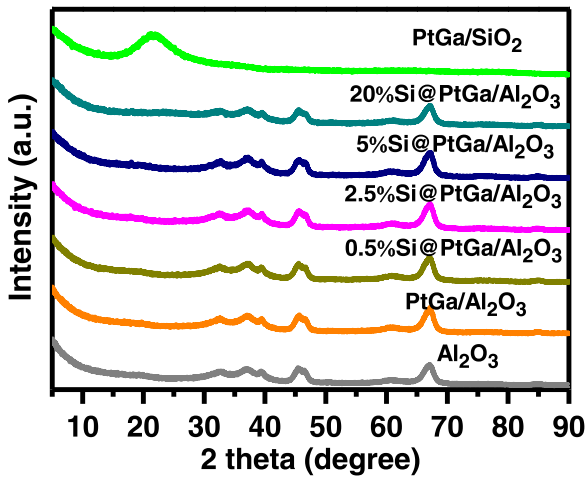

Fig. 3. The XRD patterns of the fresh catalysts.

Table 1
Textural properties and NH_3 uptake.

Sample	Porosity data				NH_3 uptake, mmol/$g_{cat.}$
	$S_{BJH,\ meso}$ [m^2/g][a]	$S_{t\text{-}Plot,\ micro}$ [m^2/g][b]	V_{meso} [cm^3/g][a]	V_{micro} [cm^3/g][b]	Total, mmol/$g_{cat.}$[c]
Al_2O_3	126	28.8	0.726	0.0125	/
$PtGa/Al_2O_3$	156	8.1	0.619	0.0030	/
0.5% Si@PtGa/Al_2O_3	146	7.8	0.557	0.0030	0.563
2.5% Si@PtGa/Al_2O_3	139	9.1	0.473	0.0035	0.719
5%Si@PtGa/Al_2O_3	133	23.7	0.455	0.0094	1.051
20%Si@PtGa/Al_2O_3	101	110.8	0.247	0.0474	1.078
$PtGa/SiO_2$	46	26.0	0.124	0.0115	/

[a] from BJH adsorption method.
[b] from t-Plot method.
[c] from NH_3 uptake.

resulting interface effectively attenuates the SMSI. Moreover, the peaks position at 557 °C appear while the content of silica increasing, which are assigned to the partial reduction of well-dispersed neutral gallium oxide clusters to the cationic Ga^+ species [50,52–55], it shows the SMSI effect further regulated by more silica coating of x%Si@PtGa/Al_2O_3 (x = 2.5, 5, 20). In comparison, when the support is pure amorphous silica, the very broad peak appears from 600 °C to 900 °C, which is ascribed to bulk Ga_2O_3 particles with different-size loosely supported over support as previous reported [51]. Furthermore, the H_2-TPR profiles of the SiO_2 and Al_2O_3 supports loading with different amount of Ga_2O_3 were also conducted for furtherly clarifying the influence of interfacial regulation on the interaction between Ga species and Al_2O_3 support (Fig. S17). Briefly, the Ga is easier to be reduced over x% Si@PtGa/Al_2O_3 catalysts, because the effect of SMSI between Ga species and Al_2O_3 support is weakened by the wrapped silica. With the increase of silica coverage, more Ga^+ species will be reduced, but it will gradually reach saturation as silica completely wrapped the catalyst.

Quantitative and qualitative analysis of the acid sites were studied by NH_3-TPD as depicted in Fig. 5(b) and Table 1. The amount of NH_3 uptake over γ-Al_2O_3, Pt/Al_2O_3, Ga/Al_2O_3 and $PtGa/Al_2O_3$ are minimum (Fig. S18a), and the introducing of supported Pt and Ga species resulting in appearing a desorption peak of strong acid sites, which may be related to the carbonaceous deposition [29]. In the case of the silica coated 0.5% $PtGa/Al_2O_3$ catalysts, the acidity increases as shown by the NH_3 desorption peak at 470 °C. The moderate acidity is caused by interface between silica and alumina (Fig. S18b) [56]. As the increasing of silica content, the amount of NH_3 desorption are increase until the 5% introduced Si is enough to cover the catalyst surface effectively to form the interface on the catalyst surface. Meanwhile, the peaks position of x %Si@PtGa/Al_2O_3 (x = 0.5, 2.5, 5, 20) moves to the higher temperature with the increase of silica content, indicating more amount of interface are generated. As previously reported that the higher acidity promotes advantageous to relatively weak coke formation [50,51,55,57–59]. In contrast, there is no visible peak appears of $PtGa/SiO_2$.

The surface chemical properties of the $PtGa/Al_2O_3$ and 2.5% Si@PtGa/Al_2O_3 are the key factors to affect their catalytic activity in PDH reaction. To elucidate the detail chemical compositions and bonding configurations of Ga, the samples were investigated by XPS. In the Ga 3d spectra (Fig. 6a–d), an asymmetry peak attributed to $Ga^{\delta+}$ species (δ < 2) appears at ~19.8 eV [58,60–62]. The high binding energy of ~24.9 eV is assigned to O2s band and the binding energy of ~22.5 eV is attributed to Ga^{3+} band [60,61]. As listed in Table 2, whether before reaction or after reaction, the content of Ga species over the $PtGa/Al_2O_3$ and 2.5%Si@PtGa/Al_2O_3 catalysts surface are almost unanimous. The content of Ga species on the catalyst surface after the reaction is significantly higher than that before the reaction, indicating the dispersion of Ga species are boosted during the reaction. The surface ratio of $Ga^{\delta+}$ species in $PtGa/Al_2O_3$ and 2.5%Si@PtGa/Al_2O_3 catalysts are about 15.3% and 18.5%, respectively, concluded that the partial Ga_2O_3 is reduced during the catalysis process and synthesis process. The low-coordinate $Ga^{\delta+}$ species are contribute to anchor the Pt sites [63]. From the Ga 2p spectra (Fig. S19), the binding energy for Ga $2p_{3/2}$ and $2p_{1/2}$ are observed at 1118 and 1145 eV, respectively [58,64,65]. No significant difference is observed between the two catalysts. The Si 2p region can be deconvoluted into Si 2p as well as Ga $3p_{1/2}$ and Ga $3p_{3/2}$ (Fig. S20). From semi-quantitative analysis of XPS, the surface molar ratio of Si/Al is 7.8% on the spent 2.5%Si@PtGa/Al_2O_3, which indicates that the silica is exited as very thin layer even less than 1 nm, coated tightly on the surface of $PtGa/Al_2O_3$. However, the amount of Pt is too low to be detected, even if Al 2p is deconvoluted (Fig. S21–22).

3.4. The discussion on the improved catalytic activity and stability

The active sites dispersion was identified by AC-TEM at atomic resolution. As a comparison, the spent 2.5%Si@Pt/Al_2O_3 catalyst was studied by AC-TEM for illustrate the Ga species assisting in dispersing of Pt (Fig. S23). It can be seen that the Pt nanoparticles are well-dispersed on the surface of the spent 2.5%Si@Pt/Al_2O_3 catalyst even without introducing of Ga, and it shows bright spots of about ~2 nm. Thus, in order to better observe the Pt sites among PtGa clusters, the spent catalyst with 0.3% Pt loading was also for observing the structure relationships of Pt active sites and Ga species. According to the Z-contrast mechanism, a single bright spot in the PtGa cluster is Pt sites, while the neighboring dark spots are Ga species (Fig. S24a–d). Meanwhile, it can be more clearly observed that the Pt sites efficiently diluted by neighboring Ga species in the bright field AC-TEM (Fig. S24e–h), forming highly dispersed Pt sites. Similarly, when the Pt loading is as low as 0.1%, the isolated Pt bright spots in the highly dispersed PtGa clusters are observed and more atomic-dispersed compared to 0.3% Pt loaded catalyst (Fig. S25d–f and Fig. 7f). Furthermore, Fig. 7(a), (b), (d) and (e) show that PtGa clusters with a diameter of less than ~2 nm are uniformly distributed on the spent $PtGa/Al_2O_3$ and 2.5%Si@PtGa/Al_2O_3 catalysts. There are no bulk crystallized metal nanoparticles are seen, demonstrating no isolated Pt active sites subjected to sintering. From Fig. S25 and Fig. 7(c), (f), the obvious difference can be seen between the two above catalysts. The PtGa clusters constrained between γ-Al_2O_3 and amorphous silica thin layers are prone to exist in the form of loosen packed assembles (Fig. 7f and Fig. S25d–f), still remaining a very good dispersion on the surface of the spent 2.5%Si@PtGa/Al_2O_3 catalysts,

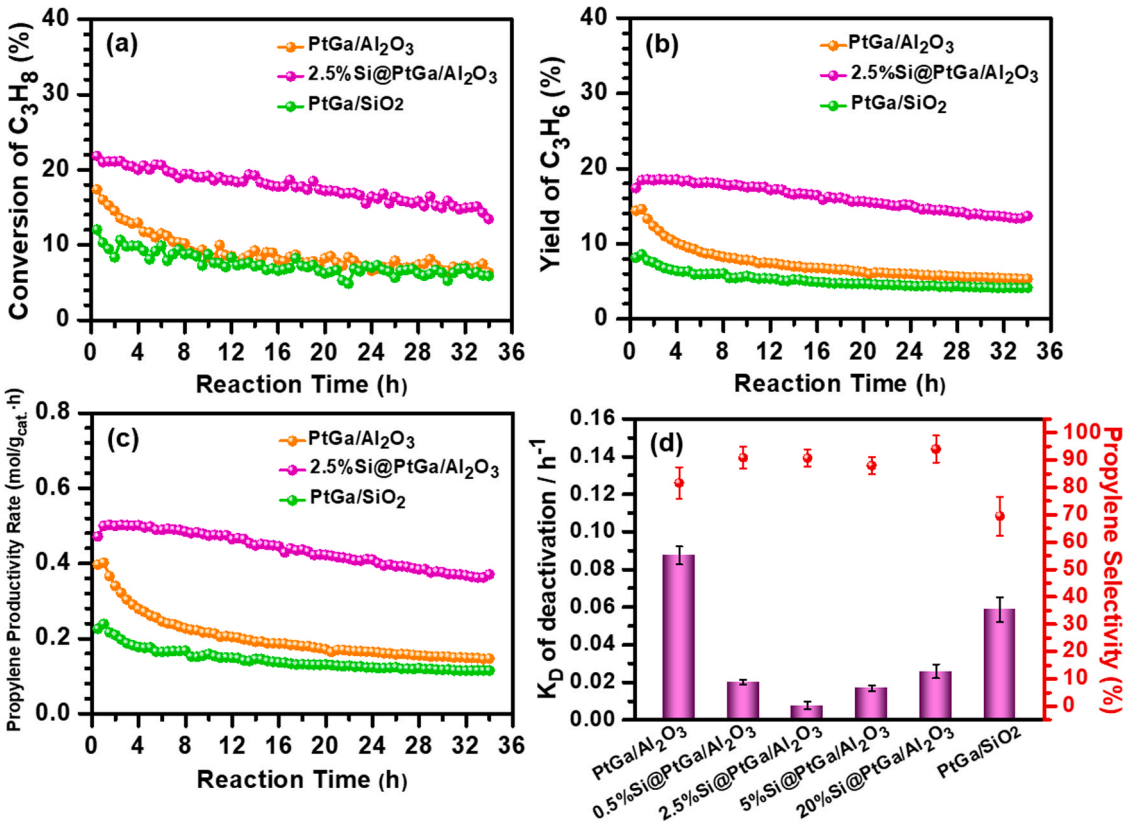

Fig. 4. Catalytic performance of different catalysts for propane dehydrogenation. (a) conversion of propane, (b) propylene yield, (c) propylene productivity rate and (d) the deactivation constant and the mean propylene selectivity of different catalysts. Catalytic test conditions: T = 450 °C, pressure= 1 bar, 100 mg of catalyst, pretreatment: Ar gas (20 mL min^{-1}) for 1 h before reaction. Reactant feed: 2.5% C_3H_8 and 2.5% H_2 with balance Ar for total flow rate of 40 mL/min.

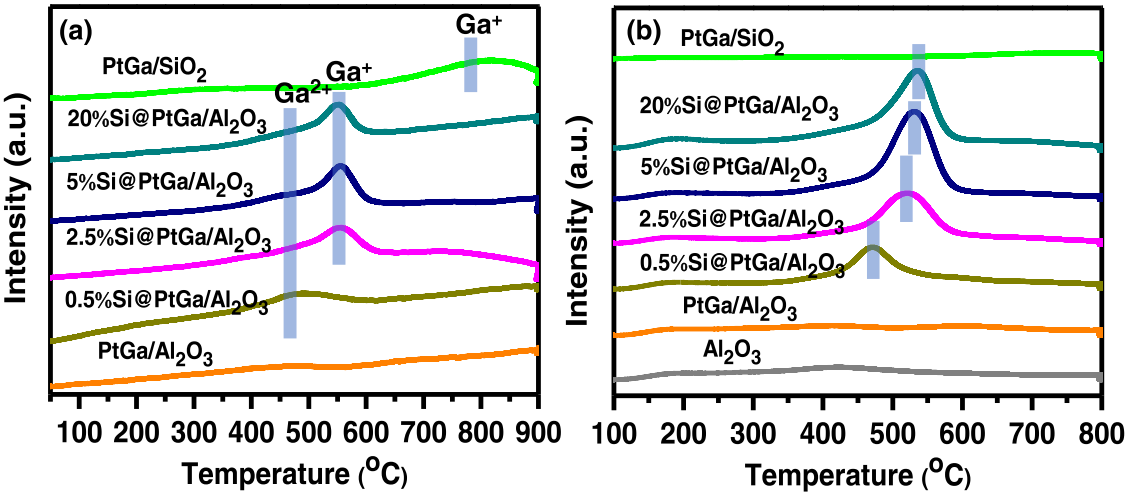

Fig. 5. Chemistry property analysis of different catalysts. (a) H_2-TPR and (b) NH_3-TPD profiles.

indicating that coating silica can efficiently restrain the PtGa clusters migration under the reaction conditions. However, for the PtGa clusters without silica coating of the prepared $PtGa/Al_2O_3$ catalyst, the structure changes significantly (Fig. 7c and Fig. S25a–c). The aggregating of Ga species on the $PtGa/Al_2O_3$ catalyst surface are existed. Moreover, there are significant amount of monodispersed atoms appeared on the surface of $PtGa/Al_2O_3$ catalyst (Fig. S26). The results indicate that coating silica thin layers can contribute to form efficient spacing to block the isolated aggregates, and the Pt active sites can be more firmly anchored on the surface of the $2.5\%Si@PtGa/Al_2O_3$ catalyst. The coordination environment of the Pt active site is relatively fixed by the interaction from PtGa clusters and silica protection. In comparison, the original PtGa clusters tend to be over agglomeration or broken without the assistance of silica coating. It is difficult to stabilize the coordination structure of Pt active sites, resulting in their significant different catalytic stability, as depicted in Fig. 8. Similarly, the XRD patterns after the reaction (Fig. S27) are consistent with those before the reaction, indicating that no macroscopic changes in the bulk phase structure of the catalyst occurred.

To clarify the influence of interfacial regulation on the electronic

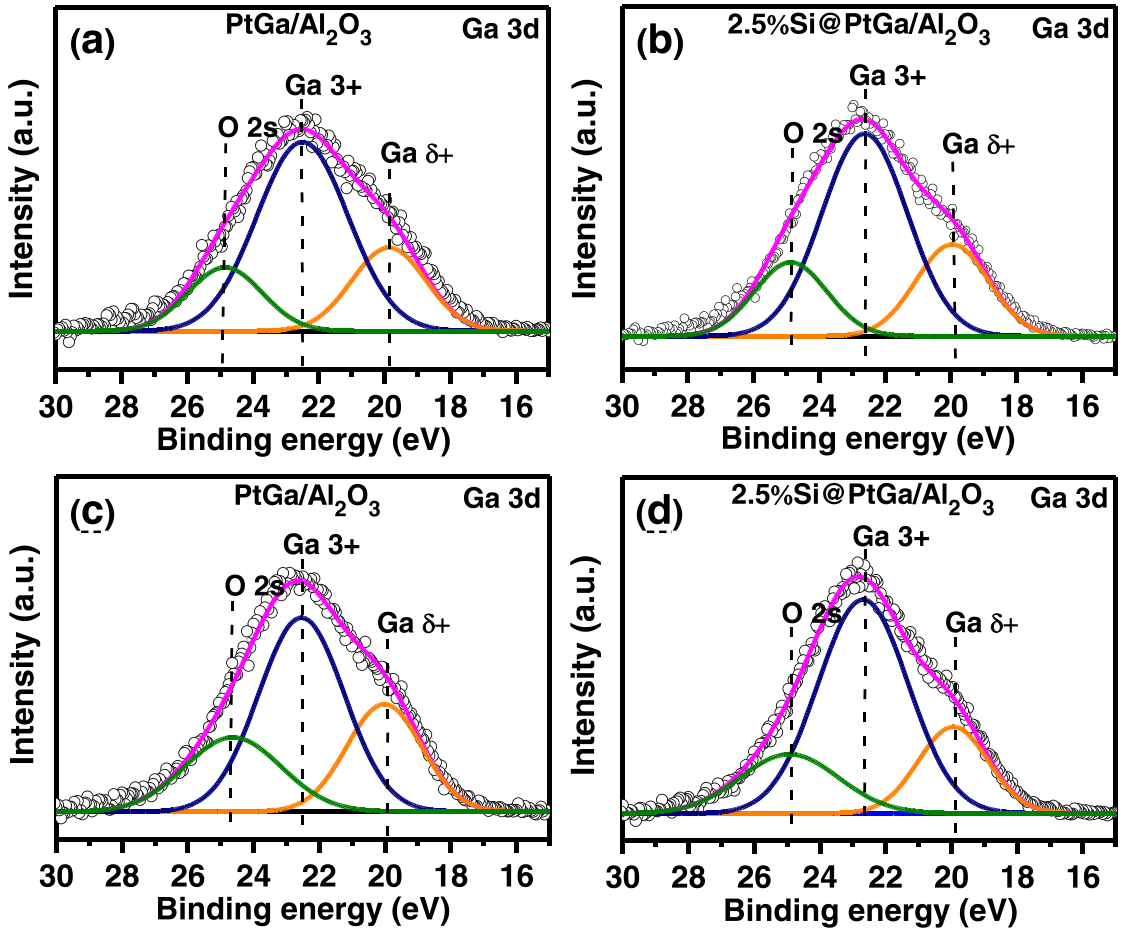

Fig. 6. XPS of Ga3d of (a-b) the fresh and (c-d) the spent catalysts.

Table 2
The semi-quantitative analysis from XPS.

Catalyst	Al 2p (at%)	Ga 3d (at%)		Si 2p (at%)
		Ga^{3+} (22.5 eV) (at%)	Ga δ^{+} ($\delta < 2$) (19.8 eV) (at%)	
$PtGa/Al_2O_3$-fresh	87.2	9.4	3.4	–
2.5%Si@PtGa/Al_2O_3-fresh	85.4	9.5	3.7	1.4
$PtGa/Al_2O_3$-used	53.4	31.3	15.3	–
2.5%Si@PtGa/Al_2O_3-used	50.6	27.6	18.5	3.3

structure of active sites on catalysts before reaction and after reaction, in situ DRIFTS was carried out with CO as the probe molecule. From Fig. S29a, it can be seen that the wavenumber of linearly adsorbed CO band of Pt/Al_2O_3 is downshifted at 2031 cm^{-1} after catalysis, indicating Pt is reduced under reaction condition, which resulting in Pt electronic density becomes higher than that of the catalyst before reaction. However, the introducing of Ga slightly shifted the vibrational frequency of the linearly bonded CO band to 2043 cm^{-1} of the spent $PtGa/Al_2O_3$ catalyst (Fig. 9b), indicating the perturbation of the electronic structure of surface Pt atoms by neighboring Ga atoms [66,67]. For comparison, the wavenumber of the CO linearly adsorbed at Pt sites over the spent 2.5%Si@Pt/Al_2O_3 catalyst is similar before and after the reaction (Fig. S29b), but it shifts to 2053 cm^{-1} due to the interfacial regulation. These results indicate that no electron transfers between silica and Pt, which is induced by Ga species. As shown in Fig. 9, compared to the fresh catalyst, the disappearing peaks at 2093 and 2121 cm^{-1} are attributed to the oxidation state of Pt and they are not conducive to dehydrogenation of propane referring to the previous literature [27, 68–70]. The remaining bands located at 2055 cm^{-1} are characteristic peaks of the linear adsorption of CO on isolated Pt sites of the spent 2.5% Si@$PtGa/Al_2O_3$. The apparent blue shift shows that the electronic structure of Pt sites is adjusted efficiently by coated with silica thin layers. Furthermore, the vibrational frequency of CO liner adsorption band of the spent 2.5%Si@$PtGa/Al_2O_3$ catalyst is still higher than that of the spent Pt/Al_2O_3 and 2.5%Si@Pt/Al_2O_3, indicating that the valence state of Pt sites is still higher than that of metallic Pt. At the same time, no peaks located at ~1820 cm^{-1} is observed over the Pt/Al_2O_3 catalyst when Pt loading as so low (Fig. S29), which is attributed to the bridge CO adsorption on the adjacent Pt atoms, suggesting too minor continuous Pt sites bonded CO to be detected. However, when the Pt loading is 0.3% and 0.5%, a bridge adsorption peak of CO appeared at 1821 and 1823 cm^{-1} (Fig. S30), but it disappears by introducing 5% Ga and only remaining the linear adsorption peak at 2046 and 2053 cm^{-1}, respectively. Because CO does not adsorb at the bridge sites between Ga and Pt, the data suggest that Ga broke the ensembles of Pt atoms on the NP surfaces and created a checkerboard Pt-Ga surface structure [67], which is consistent with the AC-TEM results. Based on the DRIFT-CO and AC-TEM results, suggesting that Ga can completely break the adjacent Pt site and form an isolated Pt site when the Pt loading is only 0.1%. Therefore, the introduced Ga leads to the dilution of Pt atoms, changing the Pt electronic properties.

When the reaction is at high temperature and anaerobic environment, coking deposition usually occurs, which will lead to the deactivation of the catalysts. To study the reasons for improved catalytic stability, the $PtGa/Al_2O_3$ and 2.5%Si@$PtGa/Al_2O_3$ were tested by

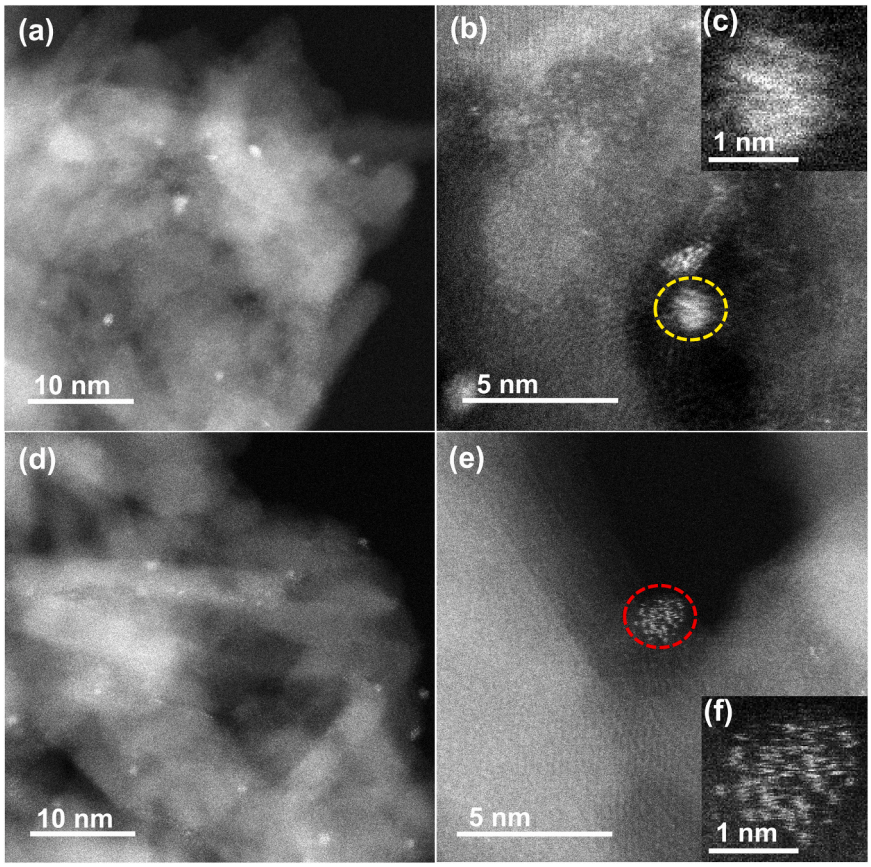

Fig. 7. (AC) HAADF-STEM images of (a–c) the spent $PtGa/Al_2O_3$ and (d–f) 2.5%Si@$PtGa/Al_2O_3$. The inset images (c) and (f) are cropped from dotted circle of images (b) and (e), respectively.

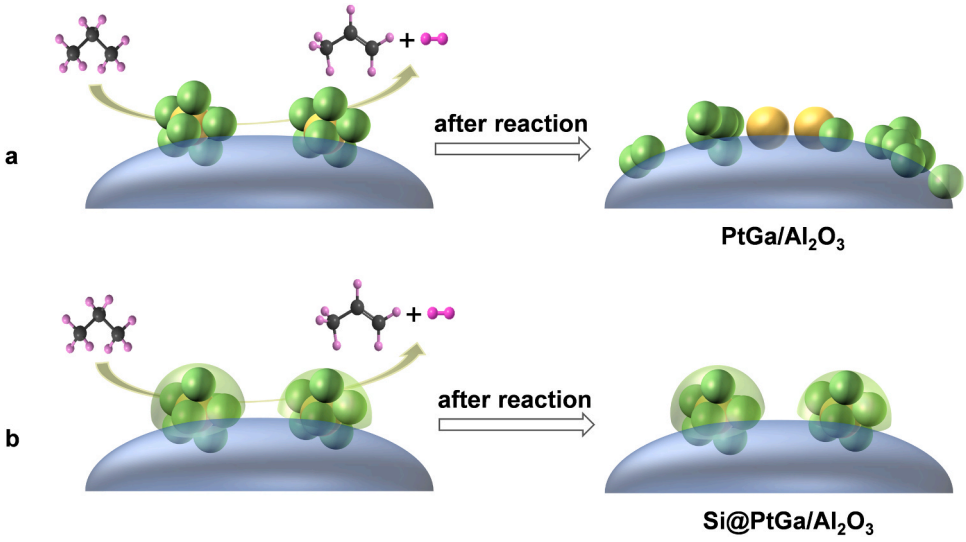

Fig. 8. Contrast diagram of the two catalysts before and after reaction. (a) $PtGa/Al_2O_3$, (b) x%Si@$PtGa/Al_2O_3$.

Raman. As shown in the Raman spectrum (Fig. S31–32), there are no obvious peaks at the location of D band and G band, which are usually used to identify the type of carbonaceous species [71]. To further identify the type of coking deposition, the spent samples were performed by TG-DSC analysis. From the Fig. 10, the weight loss curve decreases smoothly of each sample. It should be attributed to the decomposition of the adsorbed hydroxyl groups and CH_x species on the catalyst surface [71–74]. It is worth to note that the weight loss of the spent $PtGa/Al_2O_3$ is about 1.5 times as high as the spent 2.5%Si@$PtGa/Al_2O_3$, though the reaction time of $PtGa/Al_2O_3$ is only half of that of 2.5%Si@$PtGa/Al_2O_3$ catalyst. More amorphous carbon or polyaromatic substances may be formed at lower temperature (<200 °C) on the $PtGa/Al_2O_3$ catalyst [71–74]. The quantitative results show that the sample coating with amorphous silica could effectively improve the coke resistance on 2.5% Si@$PtGa/Al_2O_3$ catalyst (0.029 $mg_C/g_{Cat.}/h^{-1}$), compared to $PtGa/Al_2O_3$ (0.065 $mg_C/g_{Cat.}/h^{-1}$). Therefore, it is speculated that the

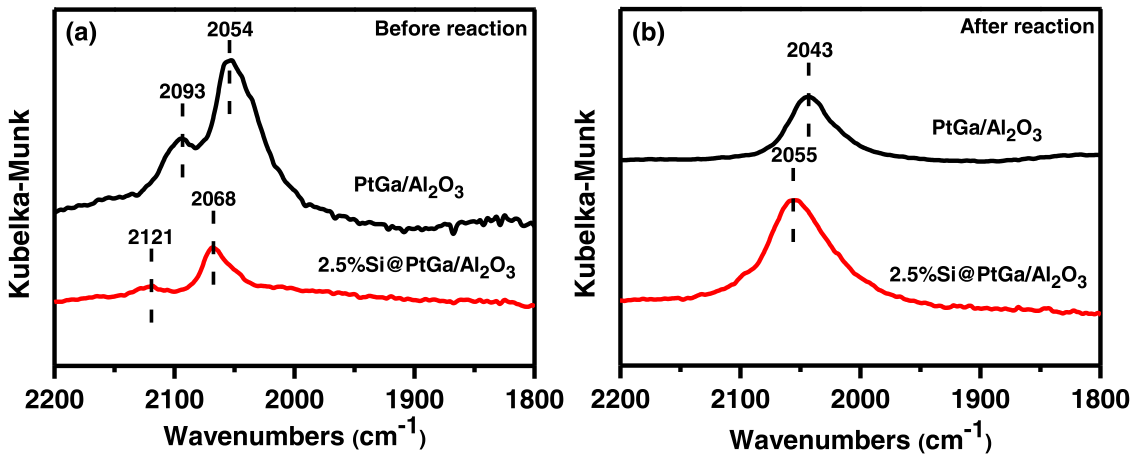

Fig. 9. DRIFT-CO of the catalysts. (a) before reaction and (b) after reaction.

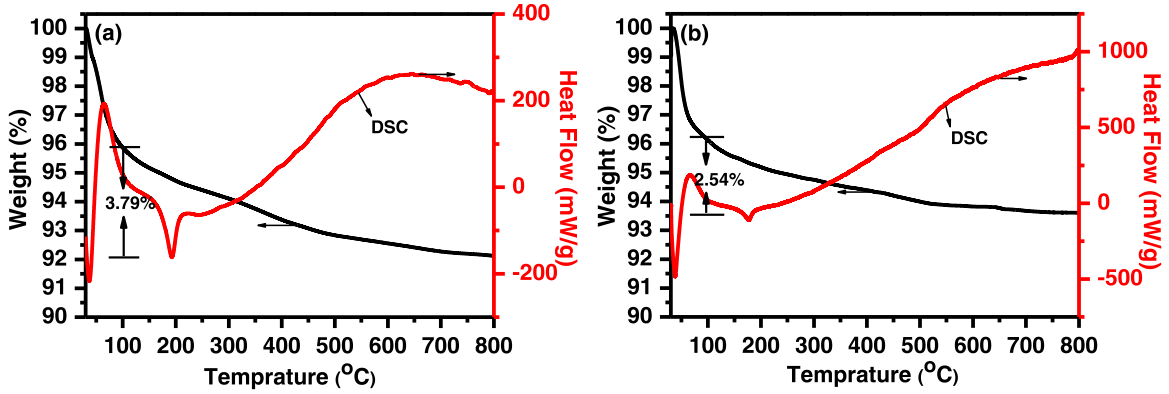

Fig. 10. TG-DSC of (a) the spent $PtGa/Al_2O_3$ and (b) $2.5\%Si@PtGa/Al_2O_3$.

very slow deactivation of the catalysts may be partly associated with the accumulation of amorphous carbon covering the surface-active species. It may be decided by whether the existence of isolated Pt active sites is stable in the catalyst structure or not.

4. Conclusions

In conclusion, this work reports a unique strategy to advance the C_3H_6 selectivity and reduce the catalyst deactivation in the PDH reaction at low temperature of 450 °C over a silica coated highly dispersed $PtGa/Al_2O_3$ catalyst. The optimal catalyst $2.5\%Si@PtGa/Al_2O_3$ with 0.1 wt% Pt loaded shows the best catalytic performance with initial propylene yield of 18.5% and 90.7% propylene selectivity. The deactivation constant of only 0.007 h^{-1} also suggests its outstanding catalyst stability. Coating silica can also profit to coke removing in the $2.5\%Si@PtGa/Al_2O_3$ catalyst, which promote its catalytic stability during the PDH reaction. The exquisite structure of $2.5\%Si@PtGa/Al_2O_3$ catalyst maximizes its catalytic performance by exposing and stabilizing isolated Pt active sites in the Ga clusters of silica and alumina interlayer. The Ga species can be more fixed at clusters state by the protection of thin silica layers in the $2.5\%Si@PtGa/Al_2O_3$ catalyst. The fixed Ga cationic clusters could change the charge distribution around Pt active sites for enhancing the PDH catalytic activity. The Pt active sites also can be anchored by the fixed Ga clusters to improve its catalytic stability during the PDH process. Briefly, this strategy provides more SMSI effect to prevent isolated Pt active sites migrating and give a stable coordination environment to Pt during the PDH catalytic process, further enhancing its catalytic performance.

Herein, it has superior potential since its outstanding economy by its atomic utilization of Pt (only 0.1 wt%), instead of the general noble metal loaded with large amount. Another advantage is that this catalyst can realize the PDH reaction with good catalytic performance near to its chemical equilibrium at the lower temperature of 450 °C rather than general 600 °C. In addition, this type of catalyst can be easily scaled up to industrial requirements in the future.

CRediT authorship contribution statement

Peng Wang: Investigation, Methodology, Formal analysis, Data curation, Validation, Writing – original draft. **Jikang Yao:** Formal analysis. **Qike Jiang:** Investigation. **Xinhua Gao:** Investigation. **Dong Lin:** Investigation. **Hua Yang:** Formal analysis. **Lizhi Wu:** Formal analysis. **Yu Tang:** Conceptualization, Supervision, Writing – review & editing, Funding acquisition. **Li Tan:** Conceptualization, Supervision, Writing – review & editing, Funding acquisition.

Declaration of Competing Interest

The authors declare that they have no known competing financial interests or personal relationships that could have appeared to influence the work reported in this paper.

Acknowledgements

This work is supported by the National Natural Science Foundation of China under grant Nos. 21902029, 21902027, 22172032, 51701201 and U19B2003, Natural Science Foundation of Fujian Province under grant Nos. 2020J05121 and 2020J01443, DNL Cooperation Fund, CAS

(DNL201903), Foundation of State Key Laboratory of High-Efficiency Utilization of Coal and Green Chemical Engineering (Grant No. 2019-KF-23).

Appendix A. Supporting information

Supplementary data associated with this article can be found in the online version at doi:10.1016/j.apcatb.2021.120731.

References

[1] C.A. Carrero, R. Schloegl, I.E. Wachs, R. Schomaecker, Critical literature review of the kinetics for the oxidative dehydrogenation of propane over well-defined supported vanadium oxide catalysts, ACS Catal. 4 (2014) 3357–3380.

[2] Y. Gu, H. Liu, M. Yang, Z. Ma, Z. Yan, Highly stable phosphine modified VO_x/Al_2O_3 catalyst in propane dehydrogenation, Appl. Catal. B: Environ. 274 (2020), 119089.

[3] T. Ren, M. Patel, K. Blok, Olefins from conventional and heavy feedstocks: energy use in steam cracking and alternative processes, Energy 31 (2006) 425–451.

[4] J.J.H.B. Sattler, J. Ruiz-Martinez, E. Santillan-Jimenez, B.M. Weckhuysen, Catalytic dehydrogenation of light alkanes on metals and metal oxides, Chem. Rev. 114 (2014) 10613–10653.

[5] S. Tan, B. Hu, W.-G. Kim, S.H. Pang, J.S. Moore, Y. Liu, R.S. Dixit, J.G. Pendergast, D.S. Sholl, S. Nair, C.W. Jones, Propane dehydrogenation over alumina-supported iron/phosphorus catalysts: structural evolution of iron species leading to high activity and propylene selectivity, ACS Catal. 6 (2016) 5673–5683.

[6] W.-D. Lu, D. Wang, Z. Zhao, W. Song, W.-C. Li, A.-H. Lu, Supported boron oxide catalysts for selective and low-temperature oxidative dehydrogenation of propane, ACS Catal. 9 (2019) 8263–8270.

[7] L. Tan, F. Wang, P. Zhang, Y. Suzuki, Y. Wu, J. Chen, G. Yang, N. Tsubaki, Design of a core-shell catalyst: an effective strategy for suppressing side reactions in syngas for direct selective conversion to light olefins, Chem. Sci. 11 (2020) 4097–4105.

[8] L. Tan, P. Zhang, Y. Cui, Y. Suzuki, H. Li, L. Guo, G. Yang, N. Tsubaki, Direct CO_2 hydrogenation to light olefins by suppressing CO by-product formation, Fuel Process. Technol. 196 (2019), 106174.

[9] Y. Dai, X. Gao, Q. Wang, X. Wan, C. Zhou, Y. Yang, Recent progress in heterogeneous metal and metal oxide catalysts for direct dehydrogenation of ethane and propane, Chem. Soc. Rev. 50 (2021) 5590–5630.

[10] S. Sokolov, M. Stoyanova, U. Rodemerck, D. Linke, E.V. Kondratenko, Comparative study of propane dehydrogenation over V-, Cr-, and Pt-based catalysts: time on-stream behavior and origins of deactivation, J. Catal. 293 (2012) 67–75.

[11] Q. Liu, M. Luo, Z. Zhao, Q. Zhao, K-modified Sn-containing dendritic mesoporous silica nanoparticles with tunable size and SnO_x-silica interaction for the dehydrogenation of propane to propylene, Chem. Eng. J. 380 (2020), 122423.

[12] L.C. Wang, Y. Zhang, J. Xu, W. Diao, D. Ding, Non-oxidative dehydrogenation of ethane to ethylene over ZSM-5 zeolite supported iron catalysts, Appl. Catal. B: Environ. 256 (2019), 117816.

[13] Y. Dai, Y. Wu, H. Dai, X. Gao, S. Tian, J. Gu, X. Yi, A. Zheng, Y. Yang, Effect of coking and propylene adsorption on enhanced stability for Co^{2+}-catalyzed propane dehydrogenation, J. Catal. 395 (2021) 105–116.

[14] M.A. Atanga, F. Rezaei, A. Jawad, M. Fitch, A.A. Rownaghi, Oxidative dehydrogenation of propane to propylene with carbon dioxide, Appl. Catal. B: Environ. 220 (2018) 429–445.

[15] K. Searles, K.W. Chan, J.A. Mendes Burak, D. Zemlyanov, O. Safonova, C. Copéret, Highly productive propane dehydrogenation catalyst using silica-supported Ga–Pt nanoparticles generated from single-sites, J. Am. Chem. Soc. 140 (2018) 11674–11679.

[16] J. Li, J. Li, Z. Zhao, X. Fan, J. Liu, Y. Wei, A. Duan, Z. Xie, Q. Liu, Size effect of TS-1 supports on the catalytic performance of PtSn/TS-1 catalysts for propane dehydrogenation, J. Catal. 352 (2017) 361–370.

[17] H. Xiong, S. Lin, J. Goetze, P. Pletcher, H. Guo, L. Kovarik, K. Artyushkova, B. M. Weckhuysen, A.K. Datye, Thermally stable and regenerable platinum-tin clusters for propane dehydrogenation prepared by atom trapping on ceria, Angew. Chem. Int. Ed. 56 (2017) 8986–8991.

[18] Y. Dai, J. Gu, S. Tian, Y. Wu, J. Chen, F. Li, Y. Du, L. Peng, W. Ding, Y. Yang, γ-Al_2O_3 sheet-stabilized isolate Co^{2+} for catalytic propane dehydrogenation, J. Catal. 381 (2020) 482–492.

[19] E. Gomez, S. Kattel, B. Yan, S. Yao, P. Liu, J.G. Chen, Combining CO_2 reduction with propane oxidative dehydrogenation over bimetallic catalysts, Nat. Commun. 9 (2018) 1398.

[20] A.J. Al Abdulghani, J.-H. Park, S.M. Kozlov, D.-C. Kang, B. AlSabban, S. Pedireddy, A. Aguilar-Tapia, S. Ould-Chikh, J.-L. Hazemann, J.-M. Basset, L. Cavallo, K. Takanabe, Methane dry reforming on supported cobalt nanoparticles promoted by boron, J. Catal. 392 (2020) 126–134.

[21] Z. Song, Q. Wang, C. Guo, S. Li, W. Yan, W. Jiao, L. Qiu, X. Yan, R. Li, Improved effect of Fe on the stable $NiFe/Al_2O_3$ catalyst in low-temperature dry reforming of methane, Ind. Eng. Chem. Res. 59 (2020) 17250–17258.

[22] Y. Wang, L. Yao, Y. Wang, S. Wang, Q. Zhao, D. Mao, C. Hu, Low-temperature catalytic CO_2 dry reforming of methane on $Ni-Si/ZrO_2$ catalyst, ACS Catal. 8 (2018) 6495–6506.

[23] B. Qiu, F. Jiang, W.-D. Lu, B. Yan, W.-C. Li, Z.-C. Zhao, A.-H. Lu, Oxidative dehydrogenation of propane using layered borosilicate zeolite as the active and selective catalyst, J. Catal. 385 (2020) 176–182.

[24] J.T. Grant, C.A. Carrero, F. Goeltl, J.M. Venegas, P. Mueller, S.P. Burt, S.E. Specht, W.P. Mcdermott, A. Chieregato, I. Hermans, Selective oxidative dehydrogenation of propane to propene using boron nitride catalysts, Science 354 (2016) 1570–1573.

[25] Y. Tang, Y. Wei, Z. Wang, S. Zhang, Y. Li, L. Nguyen, Y. Li, Y. Zhou, W. Shen, F. F. Tao, P. Hu, Synergy of single-atom Ni_1 and Ru_1 sites on CeO_2 for dry reforming of CH_4, J. Am. Chem. Soc. 141 (2019) 7283–7293.

[26] N. Taccardi, M. Grabau, J. Debuschewitz, M. Distaso, M. Brandl, R. Hock, F. Maier, C. Papp, J. Erhard, C. Neiss, Gallium-rich Pd–Ga Phases as Supported Liquid Metal Catalysts, Nature Chemistry 9 (2017) 862–867.

[27] Q. Zhang, S. Mo, J. Li, Y. Sun, M. Zhang, P. Chen, M. Fu, J. Wu, L. Chen, D. Ye, In situ DRIFT spectroscopy insights into the reaction mechanism of CO and toluene co-oxidation over pt-based catalysts, Catal. Sci. Technol. 9 (2019) 4538–4551.

[28] G. Liu, L. Zeng, Z.-J. Zhao, H. Tian, T. Wu, J. Gong, Platinum-modified ZnO/Al_2O_3 for propane dehydrogenation: minimized platinum usage and improved catalytic stability, ACS Catal. 6 (2016) 2158–2162.

[29] J.J. Sattler, I.D. Gonzalez-Jimenez, L. Luo, B.A. Stears, A. Malek, D.G. Barton, B. A. Kilos, M.P. Kaminsky, T.W. Verhoeven, E.J. Koers, M. Baldus, B.M. Weckhuysen, Platinum-promoted Ga/Al_2O_3 as highly active, selective, and stable catalyst for the dehydrogenation of propane, Angew. Chem. Int. Ed. 53 (2014) 9251–9256.

[30] J. Zhu, M.-L. Yang, Y. Yu, Y.-A. Zhu, Z.-J. Sui, X.-G. Zhou, A. Holmen, D. Chen, Size-dependent reaction mechanism and kinetics for propane dehydrogenation over Pt catalysts, ACS Catal. 5 (2015) 6310–6319.

[31] Y. Nakaya, J. Hirayama, S. Yamazoe, K.-i Shimizu, S. Furukawa, Single-atom Pt in Intermetallics as an ultrastable and selective catalyst for propane dehydrogenation, Nat. Commun. 11 (2020) 2838.

[32] Z. Xu, Y. Yue, X. Bao, Z. Xie, H. Zhu, Propane dehydrogenation over Pt clusters localized at the Sn single-site in zeolite framework, ACS Catal. 10 (2019) 818–828.

[33] L. Liu, M. Lopez-Haro, C.W. Lopes, C. Li, P. Concepcion, L. Simonelli, J.J. Calvino, A. Corma, Regioselective generation and reactivity control of subnanometric platinum clusters in zeolites for high-temperature catalysis, Nat. Mater. 18 (2019) 866–873.

[34] Q. Sun, N. Wang, Q. Fan, L. Zeng, A. Mayoral, S. Miao, R. Yang, Z. Jiang, W. Zhou, J. Zhang, T. Zhang, J. Xu, P. Zhang, J. Cheng, D.C. Yang, R. Jia, L. Li, Q. Zhang, Y. Wang, O. Terasaki, J. Yu, Subnanometer Bimetallic Platinum–Zinc Clusters in Zeolites for Propane Dehydrogenation, Angewandte Chemie International Edition 59 (2020) 19450–19459.

[35] Y. Wang, Z.-P. Hu, X. Lv, L. Chen, Z.-Y. Yuan, Ultrasmall PtZn bimetallic nanoclusters encapsulated in silicalite-1 zeolite with superior performance for propane dehydrogenation, J. Catal. 385 (2020) 61–69.

[36] J. Zhang, Y. Deng, X. Cai, Y. Chen, D. Ma, Tin assisted fully exposed platinum clusters stabilized on defect-rich graphene for dehydrogenation reaction, ACS Catal. 9 (2019) 5998–6005.

[37] L. Shi, G.M. Deng, W.C. Li, S. Miao, Q.N. Wang, W.P. Zhang, A.H. Lu, Al_2O_3 nanosheets rich in pentacoordinate $Al(^{3+})$ ions stabilize Pt-Sn clusters for propane dehydrogenation, Angew. Chem. Int. Ed. 54 (2015) 13994–13998.

[38] L.L. Long, K. Xia, W.Z. Lang, L.L. Shen, Q. Yang, X. Yan, Y.J. Guo, The comparison and optimization of zirconia, alumina, and zirconia-alumina supported PtSnIn trimetallic catalysts for propane dehydrogenation reaction, J. Ind. Eng. Chem. 51 (2017) 271–280.

[39] K. Xia, W.Z. Lang, P. Li, L. Long, X. Yan, Y. Guo, The influences of Mg/Al molar ratio on the properties of PtIn/Mg(Al)Ox catalysts for propane dehydrogenation reaction, Chem. Eng. J. (2016).

[40] H. Zhu, D.H. Anjum, Q. Wang, E. Abou-Hamad, L. Emsley, H. Dong, P. Laveille, L. Li, A.K. Samal, J.-M. Basset, Sn surface-enriched Pt–Sn bimetallic nanoparticles as a selective and stable catalyst for propane dehydrogenation, J. Catal. 320 (2014) 52–62.

[41] M. Seipenbusch, A. Binder, Structural stabilization of metal nanoparticles by chemical vapor deposition-applied silica coatings, J. Phys. Chem. C 113 (2009) 20606–20610.

[42] O.B. Belskaya, L.N. Stepanova, T.I. Gulyaeva, S.B. Erenburg, V.A. Likholobov, Zinc influence on the formation and properties of $Pt/Mg(Zn)AlO_x$ catalysts synthesized from layered hydroxides, J. Catal. 341 (2016) 13–23.

[43] S.H. Joo, J.Y. Park, C.K. Tsung, Y. Yamade, P. Yang, G.A. Somorjai, Thermally stable Pt/mesoporous silica core-shell nanocatalysts for high-temperature reactions, Nat. Mater. 8 (2009).

[44] P.M. Arnal, M. Comotti, F. Schüth, High-temperature-stable catalysts by hollow sphere encapsulation, Angew. Chem. Int. Ed. 45 (2006) 8224–8227.

[45] J. Lu, B. Fu, M.C. Kung, G. Xiao, J.W. Elam, H.H. Kung, P.C. Stair, Coking- and sintering-resistant palladium catalysts achieved through atomic layer deposition, Science 335 (2012) 1205–1208.

[46] J. Liu, S. Zhang, Y. Zhou, V. Fung, L. Nguyen, D.-e Jiang, W. Shen, J. Fan, F.F. Tao, Tuning catalytic selectivity of oxidative catalysis through deposition of nonmetallic atoms in surface lattice of metal oxide, ACS Catal. (2016) 4218–4228.

[47] S. Rimaz, L. Chen, S. Kawi, A. Borgna, Promoting effect of Ge on Pt-based catalysts for dehydrogenation of propane to propylene, Appl. Catal. A: Gen. 588 (2019), 117266.

[48] X.-Q. Gao, W.-D. Lu, S.-Z. Hu, W.-C. Li, A.-H. Lu, Rod-shaped porous alumina-supported Cr_2O_3 catalyst with low acidity for propane dehydrogenation, Chin. J. Catal. 40 (2019) 184–191.

[49] K.C. Szeto, Z.R. Jones, N. Merle, C. Rios, A. Gallo, F. Le Quemener, L. Delevoye, R. M. Gauvin, S.L. Scott, M. Taoufik, A strong support effect in selective propane dehydrogenation catalyzed by Ga(i-Bu)3 grafted onto γ-alumina and silica, ACS Catal. 8 (2018) 7566–7577.

[50] C.-T. Shao, W.-Z. Lang, X. Yan, Y.-J. Guo, Catalytic performance of gallium oxide based-catalysts for the propane dehydrogenation reaction: effects of support and loading amount, RSC Adv. 7 (2017) 4710–4723.
[51] N. Rane, M. Kersbulck, R.A. van Santen, E.J.M. Hensen, Cracking of N-heptane over brønsted acid sites and lewis acid Ga sites in ZSM-5 zeolite, Microporous Mesoporous Mater. 110 (2008) 279–291.
[52] Y. Wang, A. Caiola, B. Robinson, Q. Li, J. Hu, Hierarchical galloaluminosilicate MFI catalysts for ethane nonoxidative dehydroaromatization, Energy Fuels 34 (2020) 3100–3109.
[53] V.J. Cybulskis, S.U. Pradhan, J.J. Lovón-Quintana, A.S. Hock, B. Hu, G. Zhang, W. N. Delgass, F.H. Ribeiro, J.T. Miller, The nature of the isolated gallium active center for propane dehydrogenation on Ga/SiO_2, Catal. Lett. 147 (2017) 1252–1262.
[54] Q. Yu, T. Yu, H. Chen, G. Fang, X. Pan, X. Bao, The effect of Al^{3+} coordination structure on the propane dehydrogenation activity of $Pt/Ga/Al_2O_3$ catalysts, J. Energy Chem. 41 (2020) 93–99.
[55] X. Su, Y. Fang, X. Bai, W. Wu, Synergic effect of GaO^+/brønsted acid in hierarchical Ga/Al-ZSM-5 bifunctional catalysts for 1-hexene aromatization, Ind. Eng. Chem. Res. 58 (2019) 20543–20552.
[56] W.-g Kim, J. So, S.-W. Choi, Y. Liu, R.S. Dixit, C. Sievers, D.S. Sholl, S. Nair, C. W. Jones, Hierarchical Ga-MFI catalysts for propane dehydrogenation, Chem. Mater. 29 (2017) 7213–7222.
[57] C. Song, M.Y. Gim, Y.H. Lim, D.H. Kim, Enhanced yield of benzene, toulene, and xylene from the Co-aromatization of methane and propane over gallium supported on mesoporous ZSM-5 and ZSM-11, Fuel 251 (2019) 404–412.
[58] M. Kashif, M. Yuan, M. Abduallah, Y. Su, Fully selective catalytic oxidation of NO to NO_2 over most active Ga-PCH catalyst, J. Environ. Chem. Eng. 8 (2020), 103524.
[59] J.S. Espindola, C.J. Gilbert, O.W. Perez-Lopez, J.O. Trierweiler, G.W. Huber, Conversion of furan over gallium and zinc promoted ZSM-5: the effect of metal and acid sites, Fuel Process. Technol. 201 (2020), 106319.
[60] S. Collins, M. Baltanas, J. Garciafierro, A. Bonivardi, Gallium–hydrogen bond formation on gallium and gallium–palladium silica-supported catalysts, J. Catal. 211 (2002) 252–264.
[61] B. Xu, B. Zheng, W. Hua, Y. Yue, Z. Gao, Support effect in dehydrogenation of propane in the presence of CO_2 over supported gallium oxide catalysts, J. Catal. 239 (2006) 470–477.
[62] R. Carli, C.L. Bianchi, R. Giannantonio, V. Ragaini, Low temperature reduction of gallium in a Ga_2O_3/HZSM-5 catalyst, J. Mol. Catal. 83 (1993) 379–389.
[63] A.B. Getsoian, U. Das, J. Camacho-Bunquin, G. Zhang, J.R. Gallagher, B. Hu, S. Cheah, J.A. Schaidle, D.A. Ruddy, J.E. Hensley, Organometallic model complexes elucidate the active gallium species in alkane pehydrogenation catalysts based on ligand effects in Ga K-edge XANES, Catal. Sci. Technol. 6 (2016) 6339–6353.
[64] R. Carli, C.L. Bianchi, XPS analysis of gallium oxides, Appl. Surf. Sci. 74 (1994) 99–102.
[65] A.I. Serykh, M.D. Amiridis, In-situ X-ray photoelectron spectroscopy study of supported gallium oxide, Surf. Sci. 604 (2010) 1002–1005.
[66] A.H. Motagamwala, R. Almallahi, J. Wortman, V.O. Igenegbai, S. Linic, Stable and selective catalysts for propane dehydrogenation operating at thermodynamic limit, Science 373 (2021) 217–222.
[67] C. Li, G. Wang, Dehydrogenation of light alkanes to mono-olefins, Chem. Soc. Rev. 50 (2021) 4359–4381.
[68] H. Jeong, D. Shin, B.S. Kim, J. Bae, S. Shin, C. Choe, J.W. Han, H. Lee, Controlling the oxidation state of Pt single atoms for maximizing catalytic activity, Angew. Chem. Int. Ed. Engl. 59 (2020) 20691–20696.
[69] J. Li, Y. Tang, Y. Ma, Z. Zhang, F. Tao, Y. Qu, In situ formation of isolated bimetallic PtCe sites of single-dispersed Pt on CeO_2 for low-temperature CO oxidation, ACS Appl. Mater. Interfaces 10 (2018) 38134–38140.
[70] T. Gan, X. Chu, H. Qi, W. Zhang, Y. Zou, W. Yan, G. Liu, Pt/Al_2O_3 with ultralow Pt-loading catalyze toluene oxidation: promotional synergistic effect of Pt nanoparticles and Al_2O_3 support, Appl. Catal. B: Environ. 257 (2019), 117943.
[71] A. Iglesias-Juez, A.M. Beale, K. Maaijen, T.C. Weng, P. Glatzel, B.M. Weckhuysen, A combined In-situ time-resolved UV–Vis, Raman and high-energy resolution X-ray absorption spectroscopy study on the deactivation behavior of Pt and PtSn propane dehydrogenation catalysts under industrial reaction conditions, J. Catal. 276 (2010) 268–279.
[72] Z. Ji, D. Miao, L. Gao, X. Pan, X. Bao, Effect of pH on the catalytic performance of $PtSn/B\text{-}ZrO_2$ in propane dehydrogenation, Chin. J. Catal. 41 (2020) 719–729.
[73] S. Zhou, S. Liu, F. Jing, C. Jiang, J. Shen, Y. Pang, S. Luo, W. Chu, Effects of dopants in PtSn/M-silicalite-1 on structural property and on catalytic propane dehydrogenation performance, ChemistrySelect 5 (2020) 4175–4185.
[74] X. Niu, X. Nie, C. Yang, J.G. Chen, CO_2-assisted propane aromatization over phosphorus-modified Ga/ZSM-5 catalysts, Catal. Sci. Technol. 10 (2020) 1881–1888.